

A Current-Sensorless Digital Controller for Active Power Factor Correction Control Based on Kalman Filters

Jonathan W. Kimball, *Senior Member*
Department of Electrical and Computer Engineering
Missouri University of Science & Technology
Rolla, Missouri 65409 USA

Philip T. Krein, *Fellow*
Grainger Center for Electric Machinery and Electromechanics
Department of Electrical and Computer Engineering
University of Illinois, Urbana, Illinois 61801 USA

Abstract – For low-power ac-dc converters, power factor correction (PFC) can be accomplished simply with certain converters operating in discontinuous conduction mode (DCM). At higher power levels, DCM results in higher losses, so most PFC converters use current feedback to actively track the correct current waveshape. This work presents a way to provide PFC control without the current sensor, by replacing the sensor with a Kalman filter, which is essentially a stochastic observer. Experimental results verify its high power factor and low total harmonic distortion (THD).

I. INTRODUCTION

Power factor correction (PFC) is a widely-used technique [1] that allows an ac-dc converter to meet power quality standards, such as [2]. Low-power converters can benefit from a variety of converter topologies that automatically provide the PFC function, or controllers that exploit discontinuous conduction mode such as [3]. High power converters (e.g., more than 1 kW) are best served with methods that use current sensors, such as [4-6]. The present work targets the middle range, where the excessive losses of the low-power techniques are undesirable and the current sensor is too expensive.

A Kalman filter [7] can be used to augment or replace sensors in a noisy environment. This work uses two extended Kalman filters (EKFs) to form a current-sensorless PFC algorithm. The information needed for control purposes is derived from input and bus voltage measurements. Experimental results from a converter operating at 361 W validate the method.

II. BACKGROUND ON KALMAN FILTERS AND EXTENDED KALMAN FILTERS

A Kalman filter [7] is similar to a discrete-time observer [8]. A plant model is constructed with one or more discrete state variables and an output equation. An estimator uses the same plant model to generate estimated state variables. Feedback on the error between actual and estimated output corrects the state estimates.

The basic difference is that Kalman filters are built on stochastic assumptions, rather than deterministic assumptions. The standard plant model is

$$\mathbf{x}[k] = \mathbf{\Phi}[k-1]\mathbf{x}[k-1] + \mathbf{\Gamma}[k-1] + \mathbf{w}[k-1] \quad (1)$$

In general, \mathbf{x} is a vector of n discrete state variables with time index k . The term $\mathbf{\Phi}$ is the state transition matrix, which may be time-varying. The term $\mathbf{\Gamma}$ accumulates the effects of all known (deterministic) inputs. The last component, \mathbf{w} , is a

random process with zero mean and covariance matrix \mathbf{Q} . A Kalman filter is optimal if each sample of \mathbf{w} is Gaussian and independent. If \mathbf{w} takes some other form, a Kalman filter is still the best linear estimator.

There are two possible output equation forms that result in either conventional or extended Kalman filters. A conventional Kalman filter assumes a linear output equation,

$$\mathbf{z}[k] = \mathbf{H}[k]\mathbf{x}[k] + \mathbf{v}[k] \quad (2)$$

The output \mathbf{z} is a vector of length m . \mathbf{H} is an $m \times n$ matrix that may be time-varying. The added term, \mathbf{v} , is a random process with zero mean and covariance matrix \mathbf{R} . The two random processes \mathbf{w} and \mathbf{v} are uncorrelated. In the other system form, the output equation is nonlinear,

$$\mathbf{z}[k] = h(\mathbf{x}[k]) + \mathbf{v}[k] \quad (3)$$

If there are any system nonlinearities, the filter is termed an EKF. The filter itself is unchanged, except that the local derivative of $h(\mathbf{x})$ is needed.

$$\mathbf{H}[k] = \left. \frac{\partial h}{\partial \mathbf{x}} \right|_{\mathbf{x}=\mathbf{x}[k]} \quad (4)$$

So what are the states \mathbf{x} ? A power electronics expert might expect capacitor voltages or inductor currents to be the states. This need not be the case, though. In the examples below, the state variables are parameters that can be used to create a waveform—magnitude and phase information. Kalman filters can be considered as signal processing elements that extract useful information from noisy measurements. Kalman filter application relies on an appropriate system formulation that uses this information in a controller, which may be significantly different from a conventional observer-based system.

An EKF can be designed for the dynamical system (1), with output equation (3) and derivative matrix (4). The filter tracks the covariance of the estimator error \mathbf{P} to determine the optimal gain \mathbf{K} . At each sample, an intermediate estimate of the new estimate covariance is computed from the dynamics of the state variables.

$$\mathbf{P}^- [k] = \mathbf{\Phi}[k-1]\mathbf{P}[k-1]\mathbf{\Phi}^T [k-1] + \mathbf{Q}[k-1] \quad (5)$$

Next, the optimal gain is computed from knowledge of the output equation.

$$\mathbf{K}[k] = \mathbf{P}^- [k]\mathbf{H}^T [k](\mathbf{H}[k]\mathbf{P}^- [k]\mathbf{H}^T [k] + \mathbf{R}[k])^{-1} \quad (6)$$

The gain is used to update the state estimate $\hat{\mathbf{x}}$:

$$\hat{\mathbf{x}}[k] = \mathbf{\Phi}[k]\hat{\mathbf{x}}[k-1] + \mathbf{\Gamma}[k-1] + \mathbf{K}[k](\mathbf{z}[k] - h(\hat{\mathbf{x}}[k-1])) \quad (7)$$

Also, the error covariance is updated with the optimal gain.

$$\mathbf{P}[k] = (\mathbf{I} - \mathbf{K}[k]\mathbf{H}[k])\mathbf{P}^- [k] \quad (8)$$

Then $\hat{\mathbf{x}}$ will converge to \mathbf{x} despite the presence of noise.

Practical implementation must overcome several issues. The plant model must have suitable states whose deterministic evolution can be established. Covariance matrices \mathbf{Q} and \mathbf{R} must be estimated, often from experimental data, simulations, or simple models. The estimator error covariance matrix \mathbf{P} must be initialized to a reasonable value.

EKFs, though computationally expensive, are tractable with readily available microprocessors. In addition to matrix multiplications, there is a matrix inversion and a nonlinear function h . For the present work, two EKFs were simultaneously implemented on a Texas Instruments TMS320F2812, which is a 32-bit fixed-point digital signal processor (DSP) that can achieve 133 MIPS [9]. In the experimental system, a clock speed of 75 MHz supported a 25 kHz update rate. Designers must have an awareness of computational complexity when formulating the system. The system described below uses two separate EKFs of two and three state variables, rather than one system with five state variables, to reduce the computations required for matrix inversion.

III. APPLICATION OF AN EKF TO AC VOLTAGE SENSING

In this section, an EKF will be developed for ac voltage sensing. The end application is a PFC converter, such as the boost converter of Fig. 1. In most PFC controllers, the input voltage V_{in} is sensed after the rectifier. Sample rate is limited, and sample values are quantized. Additionally, there is significant analog noise. The objective of the EKF is to produce an estimate of the true V_{in} , so that a PFC converter will produce clean, sinusoidal input current.

A Kalman filter can be constructed to determine the true input voltage magnitude and phase in the presence of quantization and analog noise. V_{in} is modeled as a sine wave. An external circuit generates a digital signal that gives the polarity of the ac voltage. If two successive samples of this digital polarity indicator differ, then a zero crossing has occurred and time is reset to zero. However, there may be an error between the actual zero crossing and the sensed zero crossing of as much as T , the sample period. This error, called θ and measured in radians, is based on the known radian line frequency ω (for instance, $\omega = 2\pi 60$ rad/s). The output

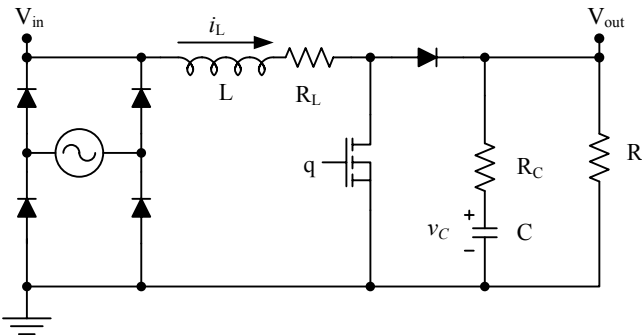


Fig. 1. Boost PFC converter.

equation is

$$V_{in}[k] = V_{pk}[k] \sin(k\omega T + \theta[k]) + v[k] \quad (9)$$

The additive noise v will be discussed later. For this form of the output equation, the relevant states are V_{pk} and θ . So the dynamical system is

$$\begin{bmatrix} V_{pk} \\ \theta \end{bmatrix} [k] = \begin{bmatrix} V_{pk} \\ \theta \end{bmatrix} [k-1] + \mathbf{w}[k-1] \quad (10)$$

The state transition matrix is the identity matrix; that is, there are no deterministic dynamics. The magnitude and phase may drift between zero crossings, though. Since the drift is nondeterministic, it can be modeled with a random variable \mathbf{w} .

There are two components to the sensed random variable v . The real value of V_{in} passes through an analog gain stage (gain G_v) which has some analog noise. Measurements of a physical system can give an indication of the magnitude of the analog noise. The noisy analog signal is then quantized by an ADC. Quantization noise can be calculated directly. The ADC has a resolution of p bits; for example, a TMS320F2812 has a 12-bit ADC. All signals must fit within the allowable input range $[0, V_{ADC}]$. So the quantization error e_q is limited to

$$-\frac{V_{ADC}}{G_v} \times \frac{1}{2^{p+1}} \leq e_q < \frac{V_{ADC}}{G_v} \times \frac{1}{2^{p+1}} \quad (11)$$

The quantization error e_q is a uniform random variable with zero mean and extents per (11), so the variance is

$$\sigma_{e_q}^2 = \frac{1}{3} \left(\frac{V_{ADC}}{2^{p+1} G_v} \right)^2 \quad (12)$$

In a typical system, analog noise dominates. A 12-bit ADC with $V_{ADC} = 2.5$ V and $G_v = 0.01$ gives a variance of 0.00031 V². Analog noise might be as much as 1% of full scale, or 2.5 V, for a variance of 6.25 V².

The other random process \mathbf{w} determines changes in V_{in} . The derivative of V_{pk} is governed by \mathbf{w}_1 . Experimentally, any small positive number used for the variance of \mathbf{w}_1 produces acceptable results, since line voltage changes over the course of minutes or hours and the sample rate is on the order of milliseconds. The angle θ is reset to its mean, $\omega T/2$, at each zero crossing. Since this time-quantization error is a uniform random variable ($\theta \in [0, \omega T]$), the corresponding term in the \mathbf{P} matrix is reset to

$$\mathbf{P}_{22} = \frac{(\omega T)^2}{12} \quad (13)$$

at each sensed zero crossing. The variance of \mathbf{w}_2 , which governs changes in θ over a cycle, must be smaller; an experimental value of $\frac{\mathbf{P}_{22}}{12}$ resulted in good performance.

This EKF was used effectively in the experimental PFC converter described in the next section. One drawback to the formulation of (9) is that harmonics are not considered. As long as the input voltage is a clean, single-frequency sinusoid, acceptable performance results.

IV. SENSORLESS PFC ALGORITHM

This section presents a new current-sensorless PFC control algorithm that only uses voltages (input and output). Computational complexity is manageable with a DSP. High power factor (0.985) and low THD (9.3%) are achieved. The power circuit is a boost converter, as shown in Fig. 1.

The controller is partitioned into a real power loop and a power factor angle loop. The real power affects the moving-average output voltage. Unity power factor corresponds to a power factor angle of zero, so the power factor angle can be used to control input current. The overall system diagram is shown in Fig. 2. The individual blocks will be discussed throughout the following subsections.

Real power can be considered in the phasor domain. For a sufficiently high switching frequency, the boost converter can be modeled as a rectified ac voltage source with rms magnitude V_{eq} and phase angle $\psi + \theta$ connected to the line through an impedance $j\omega L = jX_L$. That is, the angle between \bar{V}_{eq} and \bar{V}_{in} (in the phasor domain) is ψ . The real power into the converter is

$$P_{in} = -\frac{V_{inrms} V_{eq}}{X_L} \sin \psi \approx -\frac{V_{pk}^2}{2X_L} \psi \quad (14)$$

The magnitude V_{eq} is adjusted to maintain near-zero reactive power, so $V_{eq} \approx V_{inrms} = \frac{V_{pk}}{\sqrt{2}}$. Just as for a synchronous generator, the primary adjustment for real power is the phase angle ψ , which is small. Real power flow determines the change in output voltage, since any difference between input power P_{in} and load power P_{out} will charge or discharge the output capacitor C . The voltage across the capacitor can be partitioned into a slow-changing dc value V_{odc}

plus a zero-mean ripple voltage at twice the line frequency. Power balance only affects V_{odc} .

The nonlinear capacitor voltage dynamics of a boost converter can be linearized through a change of coordinates. Instead of V_{odc} as a state, the stored energy

$$E = \frac{1}{2} C V_{odc}^2 \quad (15)$$

is used [5, 10]. The discrete-time dynamical equation for E is linear with a sample rate of $T_{ripple} = \frac{1}{120}$ s.

$$E[k] = E[k-1] + (P_{in} - P_{out}) T_{ripple} \quad (16)$$

Linear discrete-time systems can achieve deadbeat performance. The control law is

$$\psi[k+1] = \psi[k] + \frac{1}{G} (E_{ref} - 2E[k] + E[k-1]) \quad (17)$$

$$G = -\frac{V_{pk}^2}{2\omega L}$$

E_{ref} is the reference energy, i.e., the value of E at the reference output voltage. True deadbeat performance can be achieved if there is no sensing delay and if an accurate value of V_{pk} is used to compute G . Adequate performance is achieved if V_{odc} is the output of a Kalman filter and if an approximately correct value of V_{pk} (e.g., 170 V) is used to compute G .

The other control objective is to force current to follow a sinusoidal reference, or equivalently, to force the power factor angle to zero. The ripple portion of the capacitor voltage is

$$V_{oripple} = V_{opk} \sin(2\omega t + \phi + \theta) \quad (18)$$

Again, θ is the offset determined from sensed line voltage zero crossing. If ϕ can be somehow estimated, a controller can drive ϕ to zero and achieve unity power factor. A reasonable control law is a simple discrete-time PI controller,

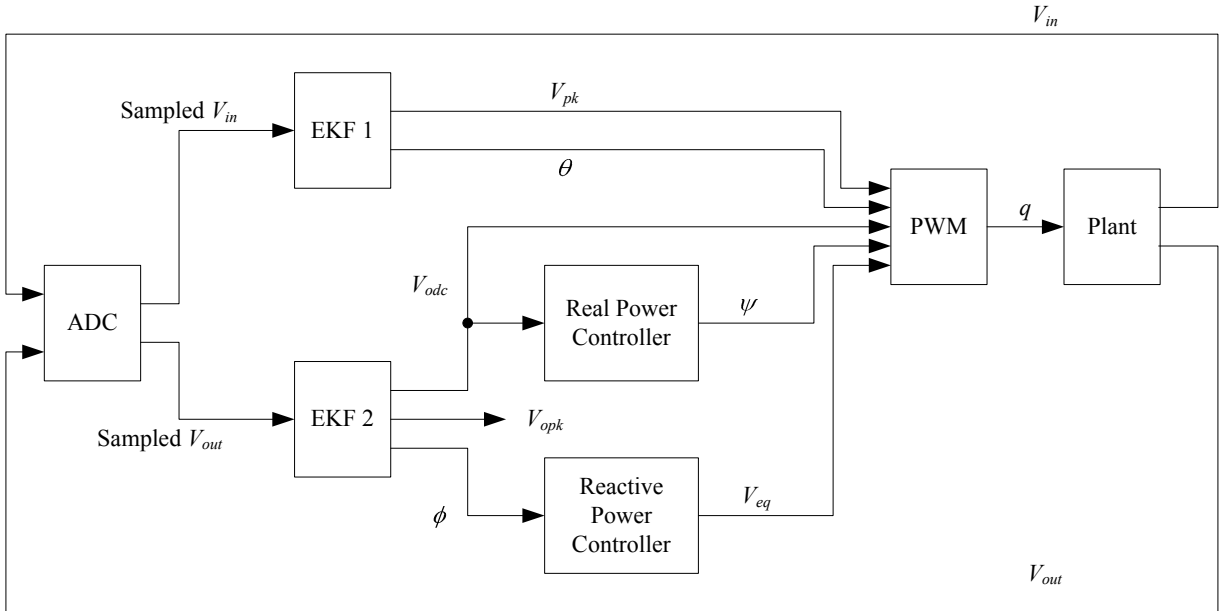


Fig. 2. Controller block diagram.

$$\begin{aligned}
V_{eq}[k] &= V_{inrms}[k] + K_p e_\phi[k] + K_I e_I[k] \\
e_\phi[k] &= \phi_{ref} - \phi[k] \\
e_I[k] &= e_I[k-1] + e_\phi[k]
\end{aligned} \tag{19}$$

The same sample rate, T_{ripple} , applies as for the real power loop. For unity power factor, $\phi_{ref} = 0$.

The basic architecture uses two control loops to regulate two portions of the output (capacitor) voltage. Real power regulates the slow-changing dc value. Reactive power regulates the power factor angle. Both loops depend on partitioned knowledge of output voltage, which can be obtained with an EKF.

V. EKF FOR VOLTAGE SENSING

The controller needs knowledge of dc and ac portions of the output voltage. As in the input voltage sensing algorithm of Section III, the output voltage can be represented by a fictitious dynamical system,

$$\begin{aligned}
\begin{bmatrix} V_{opk} \\ \phi \\ V_{odc} \end{bmatrix} [k] &= \begin{bmatrix} V_{opk} \\ \phi \\ V_{odc} \end{bmatrix} [k-1] + \mathbf{w}_o[k-1] \\
V_o[k] &= V_{opk}[k] \sin(2k\omega T + \phi[k] + \theta[k]) \\
&\quad + V_{odc}[k] + v_o[k]
\end{aligned} \tag{20}$$

The index k in (20) is updated every T , equal to the switching period. The sensing noise v_o is similar to v in (9), so similar variance applies. The random dynamics \mathbf{w}_o are affected both by the control laws, (17) and (19), and by external factors such as load changes. The covariance matrix is

$$\mathbf{Q}_{V_o} = \begin{bmatrix} \sigma_{V_{opk}}^2 & m_{2V_{opk}\phi} & m_{2V_{opk}V_{odc}} \\ m_{2V_{opk}\phi} & \sigma_\phi^2 & m_{2\phi V_{odc}} \\ m_{2V_{opk}V_{odc}} & m_{2\phi V_{odc}} & \sigma_{V_{odc}}^2 \end{bmatrix} \tag{21}$$

The variances on the main diagonal reflect changes in just one aspect of the output voltage. The covariance terms (second moments) on the off-diagonals reflect interactions between the different aspects.

Appropriate values for \mathbf{Q}_{V_o} can be estimated from limits on system transients. The magnitude of the ripple voltage depends on the load power and the bus capacitance. Suppose the rated output current is I_{dc} and the nominal bus voltage is V_{bus} . The maximum possible output power is $I_{dc}V_{bus}$. The peak of the power ripple in the capacitor is equal to the output power, at unity power factor. The ripple current, which is at twice the line frequency, has a peak amplitude

$$I_{acpk} = V_{opk} \times 2\omega C \tag{22}$$

So at maximum power,

$$V_{bus} V_{opk} \times 2\omega C = I_{dc} V_{bus} \tag{23}$$

Solving for V_{opk} , we find

$$V_{opk} = \frac{I_{dc}}{2\omega C} \tag{24}$$

Without limiting the generality of the method, the load power could change from its minimum value (zero) to its maximum

value ($I_{dc}V_{bus}$) in one zero-crossing period T_{ripple} . Typically, the changes will be much smaller. So \mathbf{w}_{o1} can be approximated as a Gaussian random variable with zero mean and standard deviation

$$\sigma_{V_{opk}} = \frac{1}{3} \frac{I_{dc}}{2\omega C} \frac{T}{T_{ripple}} \tag{25}$$

The factor of 1/3 means that a 3σ event is the maximum possible change. The last factor scales the change from the zero-crossing period to the sampling period, so that the Kalman filter may be updated more often. The standard deviation of (25) can be simplified further with

$$\omega = \frac{\pi}{T_{ripple}} \tag{26}$$

The variance needed for $\mathbf{Q}_{V_{o11}}$ is

$$\sigma_{V_{opk}}^2 = \left(\frac{I_{dc} T}{6\pi C} \right)^2 \tag{27}$$

Similar analysis applies to the other diagonal terms. Given some ϕ_{max} (typically about 0.1 rad, if the controller is operating properly),

$$\sigma_\phi^2 = \left(\frac{\phi_{max} T}{3T_{ripple}} \right)^2 \tag{28}$$

Power balance in the capacitor gives

$$\sigma_{V_{odc}}^2 = \left(\frac{I_{dc} T}{3C} \right)^2 \tag{29}$$

With basic knowledge of operational limits, the main diagonals of \mathbf{Q}_{V_o} are approximated.

The covariance terms, the off-diagonal elements of \mathbf{Q}_{V_o} , are poorly defined, as they depend on the operational scenario. For example, for a step increase in load current, V_{odc} will decrease and V_{opk} will increase; ϕ may or may not change. If the controller causes the power factor angle to shift from lagging towards unity, ϕ will decrease and V_{opk} will decrease; V_{odc} may or may not change. If the controller causes a positive power imbalance, V_{odc} will increase and V_{opk} will increase; ϕ may or may not change. Many more scenarios are possible with unknown effects on the three variables.

The covariances are related to the variances, that is,

$$m_{2V_{odc}V_{opk}} \propto \sigma_{V_{odc}} \sigma_{V_{opk}} \tag{30}$$

and so forth. The constant of proportionality depends on the dynamics of the system and the external disturbances, and must fall within the interval [-1,1]. Since the external factors are unknown, nearly any proportionality is defensible. The experimental system used

$$\mathbf{Q}_{V_o} = \begin{bmatrix} \sigma_{V_{opk}}^2 & 0.1\sigma_{V_{opk}}\sigma_\phi & -0.1\sigma_{V_{opk}}\sigma_{V_{odc}} \\ 0.1\sigma_{V_{opk}}\sigma_\phi & \sigma_\phi^2 & 0.1\sigma_{V_{odc}}\sigma_\phi \\ -0.1\sigma_{V_{opk}}\sigma_{V_{odc}} & 0.1\sigma_{V_{odc}}\sigma_\phi & \sigma_{V_{odc}}^2 \end{bmatrix} \tag{31}$$

These values gave the best overall experimental performance.

The complete control system is shown in Fig. 2. EKF1 is based on (9)-(13). EKF2 is based on (20)-(31). The real power controller, which regulates output voltage, is given by (17). The reactive power controller, which ensures unity

power factor, is given by (19). The PWM block divides the instantaneous output voltage command by the bus voltage to find duty cycle. The DSP has a hardware PWM module that creates the switching waveform q from the duty cycle command. The plant is the boost converter plus interface circuits.

VI. EXPERIMENTAL SENSORLESS PFC

The control algorithm and EKF are both built on many assumptions about input voltage, load type, and converter dynamics. First a simulation was constructed to verify proper control. As expected, the simulation worked well. However, a simulation cannot adequately capture the randomness of the physical system. That is, the simulation can include modeled random processes, but the models may not be accurate.

An experimental boost PFC converter was built to verify the model accuracy and control effectiveness. The basic framework relied on the modular inverter previously built by a

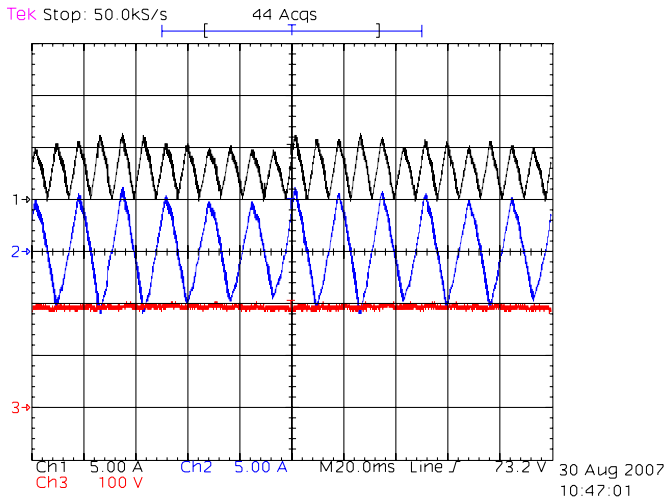


Fig. 3. Oscilloscope of experimental sensorless PFC. Top waveform, channel 1, inductor current, 5 A/div; middle waveform, channel 2, line current, 5 A/div; bottom waveform, channel 3, bus voltage, 100 V/div; horizontal scale 20 ms/div.

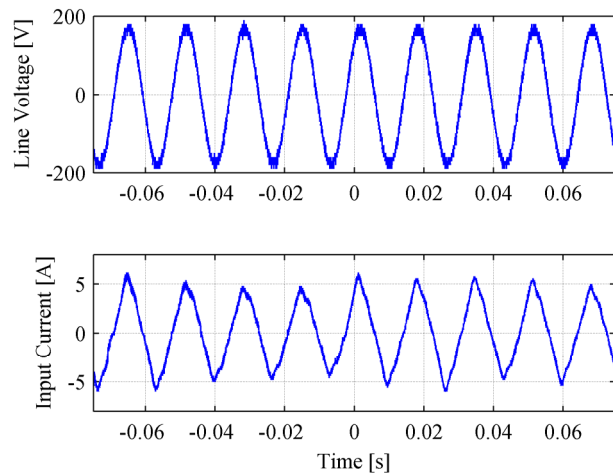


Fig. 4. As in Fig. 3, zoomed, with line voltage.

TABLE 4.1. EXPERIMENTAL CONVERTER PARAMETERS.

Main Switch	STW20NK50
Fast Diode	HFA25PB60
Inductance	3 mH
Capacitance	1800 μ F
Parasitic Resistance R_L	1.33 Ω
Capacitor Resistance R_C	0.11 Ω
Input Voltage (Nominal)	120 V
Output Voltage	190 V
Switching Frequency	25 kHz

team of graduate students [11]. The front-end active rectifier in the original modular inverter was designed for three-phase 208 V, so a new front-end section was built with hardware appropriate for single-phase PFC. Power components are listed in Table 1. The nominal output rating is 6 A (1140 W). Several tests were performed with resistive loads.

In general, performance improved with increased load. At light loads (below 0.5 A), the bus voltage ripple was too small to be reliably detected. The converter oscillated between relatively large, sinusoidal currents and zero current due to overvoltage. At moderate loads, the system performed as expected although some oscillation was observed in the magnitude of the line current. Figures 3-4 show experimental performance with a 100 Ω (1.9 A or 361 W) load. Figure 5 shows the harmonic spectrum of the line current, from a fast Fourier transform of the sampled data in Fig. 3. The total power factor is 0.985. The total harmonic distortion (THD) is 10.6%. Figure 5 also shows IEC limits [2] for class D equipment—the most stringent.

The Kalman filters were constructed with the covariance matrices described above. The deadbeat voltage control gain of (17) was used, with an approximate value of 170 V substituted for the real (sensed) V_{pk} . In the PI controller of (19), $K_p = 10$ and $K_i = 0.2083$. Larger gains produced unacceptable oscillatory behavior.

The oscillation evident in Figs. 3-4 results from residual sensed noise. The Kalman filter attenuates, rather than eliminates, quantization effects. The voltage control loop has

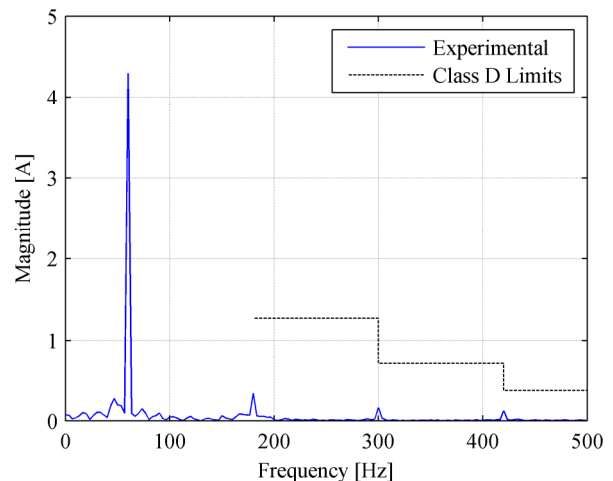


Fig. 5. Harmonic spectrum (FFT) of line current from Fig. 3, with IEC class D limits shown.

high gain, so the residual noise causes random fluctuations in the line current magnitude. The designer must trade this oscillatory behavior against the need for fast transient response. PFC voltage loop stability was the topic of [12], though much of that work used continuous-time concepts and assumed a time scale faster than T_{ripple} .

Overall, the sensorless PFC controller is stable and robust. Although there is no current sensor, near-unity power factor is achieved, and harmonic currents are lower than regulatory limits by about a factor of three.

VII. CONCLUSIONS

Kalman filters were explored in the context of voltage sensing, both for pure ac waveforms and for dc+ac waveforms. A combination of two EKFs was implemented on a DSP as the basis for a sensorless PFC algorithm. The new algorithm achieved high power factor (0.985) and low THD (10.6%).

Kalman filters can also be used for many other power electronics applications, such as parameter or load estimation in a dc-dc converter. The framework shown here uses fictitious dynamical systems to model parameterized waveshapes. Rather than estimating traditional state variables, the proposed systems estimated magnitude and phase information.

ACKNOWLEDGMENTS

This work was supported by the National Science Foundation under grant ECS 06-21643, and by the Grainger Center for Electric Machinery and Electromechanics.

REFERENCES

- [1] B. Singh, B. N. Singh, A. Chandra, K. Al-Haddad, A. Pandey, and D. P. Kothari, "A review of single-phase improved power quality ac-dc converters," *IEEE Trans. Ind. Electron.*, vol. 50, pp. 962-981, Oct. 2003.
- [2] Int. Electrotechnical Commission, "Electromagnetic compatibility (EMC) - Part 3-2: Limits - Limits for harmonic current emissions (equipment input current <16 A per phase)," Standard IEC 61000-3-2, 2001.
- [3] Z. Lai, K. M. Smedley, and Y. Ma, "Time quantity one-cycle control for power-factor correctors," *IEEE Trans. Power Electron.*, vol. 12, pp. 369-375, March 1997.
- [4] A. Prodić, J. Chen, D. Maksimović, and R. Erickson, "Self-tuning digitally controlled low-harmonic rectifier having fast dynamic response," *IEEE Trans. Power Electron.*, vol. 18, pp. 420-428, Jan. 2003.
- [5] A. H. Mitwalli, S. B. Leeb, G. C. Verghese, and V. J. Thottuvellil, "An adaptive digital controller for a unity power factor converter," *IEEE Trans. Power Electron.*, vol. 11, pp. 374-382, March 1996.
- [6] S. Chattopadhyay, V. Ramanarayanan, and V. Jayashankar, "A predictive switching modulator for current mode control of high power factor boost rectifier," *IEEE Trans. Power Electron.*, vol. 18, pp. 114-123, Jan. 2003.
- [7] A. Gelb, ed., *Applied Optimal Estimation*. Cambridge, MA: The MIT Press, 1974.
- [8] J. L. Willems, "Design of state observers for linear discrete-time systems," *Int. J. Syst. Science*, vol. 11, pp. 139-147, Feb. 1980.
- [9] Texas Instruments, "C2000 controllers overview," Sept. 23, 2006, <http://focus.ti.com/dsp/docs/dspplatformscontenttp.jsp?sectionId=2&familyId=110&tabId=510>.
- [10] D. K. Jackson and S. B. Leeb, "A digitally controlled amplifier with ripple cancellation," *IEEE Trans. Power Electron.*, vol. 18, pp. 486-494, Jan. 2003.
- [11] M. Amrhein, J. W. Kimball, A. Kwasinski, J. T. Mossoba, B. Nee, Z. Sorchini, W. Weaver, J. R. Wells, and G. Zhang, "Modular inverter for advanced control applications," University of Illinois at Urbana-Champaign, Technical Report UILU-ENG-2006-2504, CEME-TR-06-01, 2006.
- [12] A. Prodić, "Compensator design and stability assessment for fast voltage loops of power factor correction rectifiers," *IEEE Trans. Power Electron.*, vol. 22, pp. 1719-1730, Sept. 2007.